Macromolecular Rapid Communications

Macromolecular Rapid Communications
www.mrc-journal.de

RESEARCH ARTICLE OPEN ACCESS

4D Printable Formulations of Mixed Low and High Molecular Weight Liquid Crystalline Units: A Versatile Route to Functional Soft Actuators

Lorena Ceamanos[1] | María López-Valdeolivas[1] | Pengrong Lyu[2,3] | Danqing Liu[2,3] | Dirk J. Broer[2,3] | Carlos Sánchez-Somolinos[1,4]

[1]Instituto de Nanociencia y Materiales de Aragón (INMA), Departamento de Física de La Materia Condensada, CSIC-Universidad De Zaragoza, Zaragoza, Spain | [2]Human Interactive Materials Group, Department of Chemical Engineering and Chemistry, Eindhoven University of Technology, Eindhoven, The Netherlands | [3]Institute of Complex Molecular Systems, Eindhoven University of Technology, Eindhoven, The Netherlands | [4]Centro de Investigación Biomédica en Red de Bioingeniería, Biomateriales y Nanomedicina (CIBER-BBN), Instituto de Salud Carlos III, Madrid, Spain

Correspondence: Carlos Sánchez-Somolinos (carlos.s@csic.es)

Received: 3 November 2025 | **Revised:** 3 February 2026 | **Accepted:** 4 February 2026

Keywords: 4D printing | liquid crystalline polymers | reactive mesogens | responsive actuators | soft robotics

ABSTRACT

Over the last few years, 4D printing of liquid crystal elastomers (LCEs) has been explored to develop actuators with significant, reversible, and anisotropic shape changes upon external stimuli such as heat or light. Most reported ink formulations rely on photo-curable liquid crystal materials derived from high molecular weight (MW) main-chain macromers. Their rheological properties allow to program molecular alignment during direct ink writing. In contrast, formulations composed mainly of monoacrylate or diacrylate low MW mesogens are unsuitable for extrusion-based 4D printing as they fail to promote mesogen alignment during printing. This shortcoming restricts the range of chemical and physical compositions accessible to 4D printing. Here, we introduce a practical route for formulating 4D printable inks that integrate low MW mesogens. By adding an acrylate-ended macromer to the low MW constituents, these mixtures become suitable for direct ink writing. This enables the preparation of multi-functional actuators with digitally controlled director morphology and tailored properties, for example, stiffness and actuation strain, as well as light-responsive behavior when photoactive molecules are used. These results highlight the versatility of the method and suggest its potential compatibility with other functional low MW units, such as those responsive to electrical or pH stimuli.

1 | Introduction

Direct ink writing (DIW) is an additive manufacturing technique based on the extrusion and precise digital deposition of a viscoelastic ink into successive layers to create a 3D object [1, 2]. When stimuli-responsive materials are combined with this technique, the resulting structures can change their shape upon excitation with an adequate external stimulus, adding time as a fourth dimension and bringing the concept of 4D printing to the scene [3]. In this direction, in recent years, liquid crystal elastomers (LCEs), which display large, reversible, and anisotropic shape changes upon appropriate stimulation [4–7], have been combined with additive manufacturing techniques, enabling the digital programming of the mechanical response of printed liquid crystalline (LC) elements [8–15]. As a result, complex LCE structures with well-defined and reversible on-

Abbreviations: LC, liquid crystal; LCE, liquid crystal elastomer; MW, molecular weight; DIW, direct ink woriting; DSC, differential Scanning Calorimetry; DMA, dynamic Mechanical Analysis; POM, polarized optical microscopy; LED, light Emitting Diode; COP, cyclic olefin polymer..

demand shape-morphing capabilities have been achieved. 4D printed LCE actuators have been demonstrated to effectively perform translation [8–10, 16], rotation [10, 17], bending [18, 19] or squeezing [10] functions when subjected to thermal [10, 12], light [15, 19–24], magnetic [25–27] or electrical stimuli [28, 29]. These capabilities open new opportunities in medicine, adaptive optics, and soft robotics. [18, 30–36] To undergo such mechanical deformations, the rod-like molecules of the LC material need to be aligned along a preferential axis, which, in DIW, is defined by the shear and elongational flows that take place during the extrusion and deposition of the material [37]. Various LC inks have been developed in the literature, successfully inducing alignment by extrusion printing techniques. This alignment is largely influenced by the rheological properties of high molecular weight (MW) LC macromers [38, 39]. Predominantly, acrylate-ended main-chain liquid crystalline macromers have been employed, typically synthesized by a Michael addition reaction between a low MW mesogenic diacrylate and an isotropic dithiol or an amine [8, 10, 12, 40–42]. The reaction to synthesize these macromers is characterized by its simplicity and high control of the polymer structure. After printing, a second independent light-induced photopolymerization step can be triggered when a suitable photoinitiator is added to the formulation. This last photopolymerization step leads to the crosslinking of the polymer chains, fixing the molecular order induced during ink deposition [43].

In contrast, a large body of earlier LC-based actuator research relies on low MW reactive mesogens, aligned by surface-enforced techniques, magnetic fields, and electric fields [44–48]. Later, polymerization is generally initiated, enabling the formation of the polymer network from the aligned reactive mesogens. These materials can be tailored with considerable versatility, allowing the control of their properties depending on the mesogens included into the formulation. For instance, mesogenic diacrylates create highly crosslinked systems with higher stiffness, while monoacrylates soften the material and introduce additional functionalities [5, 46, 49–53]. However, in Michael addition–based step-growth systems, monoacrylates act as chain stoppers: once incorporated, they terminate the growing chain rather than extending it, thereby disrupting main-chain formation and preventing the subsequent development of a polymer network. This severely narrows the chemical design space for DIW-based 4D printing, limiting the creation of actuators with tunable properties or multifunctional responses. This highlights a clear gap in the field: while low MW mesogens offer exceptional chemical versatility and functionality, they remain largely incompatible with extrusion-based 4D printing, which predominantly relies on high MW macromers to achieve printability and molecular alignment. To date, no general strategy has been reported that bridges this gap by enabling the integration of functional low MW mesogens into DIW-printable inks while preserving molecular alignment and printability.

Here, we introduce a versatile approach that directly addresses this gap for creating functional liquid crystalline 4D printable inks using blends of high MW acrylate-ended main-chain macromers and low MW mesogenic monomers. Our strategy bridges the gap between surface-aligned low MW systems and DIW-printable high MW macromers, unlocking a broader palette of compositions for 4D printing. We hypothesize that the main-chain macromers within the mixture can play a key role in facilitating alignment during the printing process. From a rheological perspective, these high MW macromers provide the viscoelastic response required to sustain shear and elongational stresses during extrusion, which are known to promote liquid crystal alignment in direct ink writing. [8–10] In addition, the structural similarity and mesogenic character of the low and high MW constituents are expected to promote cooperative intermolecular interactions, enabling the low MW mesogens to follow the orientation imposed by the high MW macromer during printing. Photopolymerization can be used to fix this orientation afterwards, leading to a crosslinked LC system with digitally defined director (i.e., molecular alignment programmed by the printing path during direct ink writing). Crucially, low MW monomers provide a powerful means to tune final physical properties and introduce functionalities that remain largely inaccessible to extrusion-printed macromer-only inks. To validate these hypotheses and to demonstrate the potential of this approach, we have designed and formulated several 4D printable compositions integrating high MW macromers synthesized by Michael addition reaction, and low MW reactive monomers, resulting in LC actuators that respond to both heat and light as a proof of concept.

2 | Printable Thermoresponsive Model Inks based on Mixed Low/High Molecular Weight Constituents

To test the hypothesis that high MW macromers can facilitate the alignment of low MW mesogens during DIW, we designed a first set of thermoresponsive model inks. For this purpose, we selected a well-known model reactive mesogen, 1,4-Bis-[4-(6-acryloyloxyhexyloxy) benzoyloxy]-2-methylbenzene, commonly known as C6M or RM82. This was used both as a reactive monomer and as the structural LC unit of the synthesized macromer. This choice sought to favor miscibility and to provide a clear framework to study how the ratio of high and low MW constituents influences processability, thermal response, and actuation.

The macromer was synthesized through the aza-Michael addition reaction of a mesogenic diacrylate, RM82, and n-butylamine in a 1.02:1 molar ratio. The resulting macromer exhibited an average molecular weight (Mw) of 8400 $g \cdot mol^{-1}$ with a polydispersity index (PDI) of 2.1, as determined by Gel Permeation Chromatography (GPC) (see Figure S1). This macromer, the high MW constituent, was then blended with RM82 monomer, acting as the low MW constituent (Figure 1a), giving rise to a series of compositions with macromer contents of 25, 50, 75, and 90 wt.%, as outlined in Table S1. These model inks are referred to as $25_{MAC}75_{RM82}$, $50_{MAC}50_{RM82}$, $75_{MAC}25_{RM82}$, and $90_{MAC}10_{RM82}$, respectively. A formulation containing only the macromer (100 wt.%), denoted as $100_{MAC}0_{RM82}$ (Table S1), was also prepared for reference purposes [10]. In all cases, 3 wt.% of photoinitiator (Irgacure 819) was added to enable light-induced polymerization after printing.

Having established the formulations, we first investigated their phase behavior by Differential Scanning Calorimetry (DSC) (Table S1 and Figure S2). Analyses were performed without

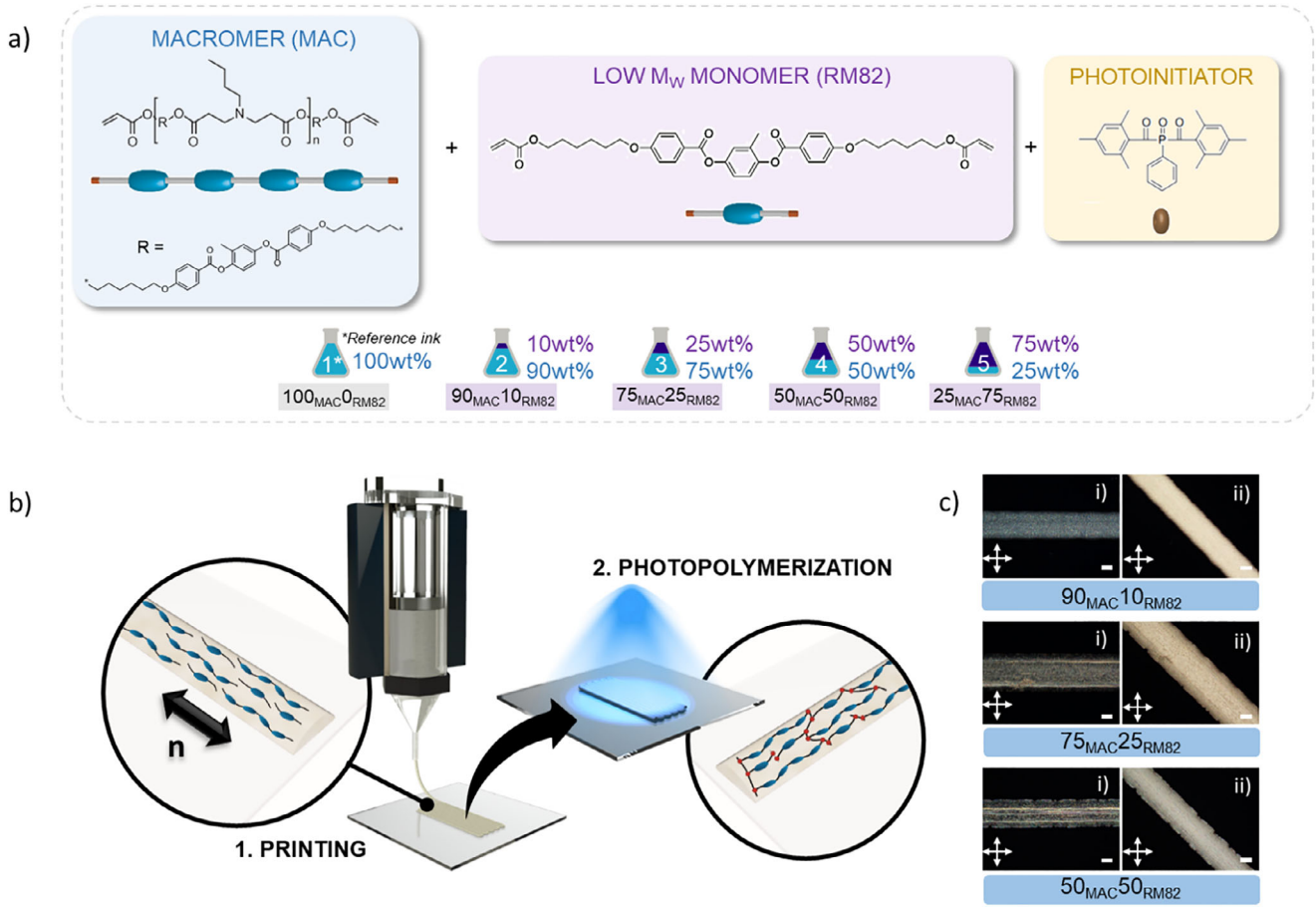

FIGURE 1 | 4D printable model inks for thermoresponsive LC actuators. (a) Molecular constituents and relative concentrations of the high MW macromer (aza-Michael addition with RM82 and n-butylamine) and low MW monomer (RM82). (b) Conceptual representation of the two main steps for manufacturing the LC samples. First, a printing step imposes the orientation of the mesogens through shear and elongational forces along the printing direction. Second, light-triggered photopolymerization takes place to obtain the LC crosslinked systems. (c) POM images of printed lines using the model inks that showed good printability (50 to 90 wt.% of macromer content). Lines are observed between crossed polarizers (crosses indicate polarizer transmission directions) with the printing direction oriented (i) parallel and (ii) at 45° to the first polarizer transmission direction (scale bar of 100 μm).

the photoinitiator to avoid its potential thermal degradation at high temperatures during thermal cycling. For the reference material with 100 wt.% of macromer content, the liquid crystal to isotropic transition temperature ($T_{LC\text{-}I}$) was identified at 104°C. This polymer is known to present a nematic phase below its transition temperature to the isotropic phase [8]. In comparison, the inks based on a mixture of the high MW main-chain macromer and the low MW monomer constituent present higher $T_{LC\text{-}I}$, shifting toward higher temperatures as the low MW content increases (Table S1), while T_g decreases accordingly, which can be tentatively attributed to a plasticization-like effect of the low MW mesogens that increases segmental mobility in the blend. $T_{LC\text{-}I}$ values obtained were 104°C, 107°C, 112°C and 115°C for the inks $90_{MAC}10_{RM82}$, $75_{MAC}25_{RM82}$, $50_{MAC}50_{RM82}$ and $25_{MAC}75_{RM82}$, respectively. This shift in $T_{LC\text{-}I}$ can be understood considering the differences in the $T_{LC\text{-}I}$ of the two pure mesogenic components of the blend. While the transition from the liquid crystal to isotropic phases occurs at 116°C for pure RM82 [54], the macromer shows a clearing temperature of about 104°C, as mentioned above. Importantly, for processing purposes, samples kept in the temperature range of 55°C to 70°C over several hours showed no phase segregation, a condition suitable for extrusion printing (vide infra).

Next, we examined the printability of these inks. Printability is understood here as the ability to generate, through extrusion, precisely deposited fibers with molecular alignment following the direction defined by the movement of the needle relative to the printing table, as previously described in the literature (Figure 1b) [10, 37, 42]. Prior to each printing cycle, inks, loaded into the printhead, were pre-heated at 87°C, within the mesophase temperature range of the two LC components, for 10 min. This ensured proper blending of components and erased thermal history. Heating to higher temperatures was avoided to prevent undesired thermal-induced alterations of the photoinitiator. Then, printing parameters such as needle diameter, printing speed, pressure, and temperature of the printhead and substrate were explored to obtain molecularly aligned printed LC morphologies (Table S2).

Continuous lines with a net molecular alignment in the direction of the needle movement were successfully printed for the inks with a macromer content of 50 wt.% or higher, demonstrating the suitability of these formulations for 4D printing (Figure 1c). Subsequently, dog-bone geometries were printed with these inks and photopolymerized into LC crosslinked systems. These LC-based actuators have a central test area of 15x3 mm and a net alignment of the molecules parallel to the longitudinal axis of

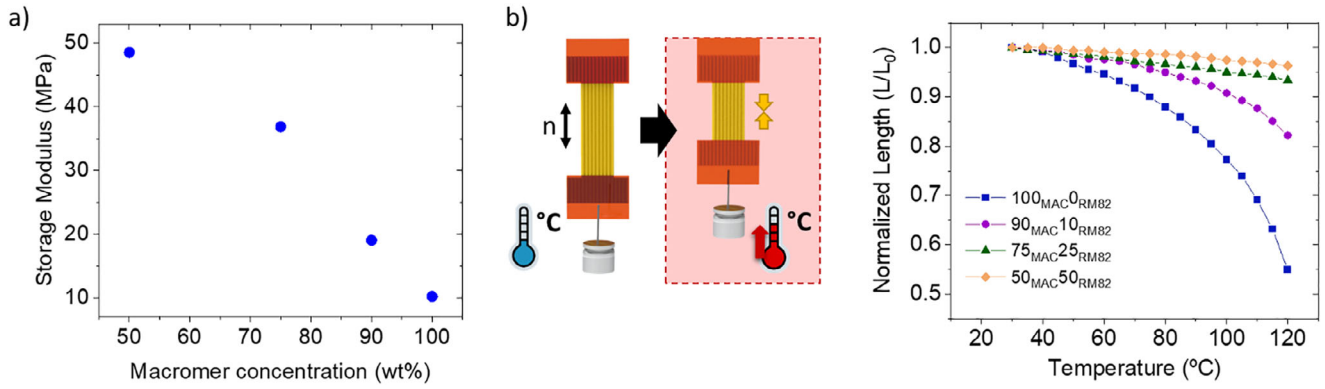

FIGURE 2 | Thermomechanical characterization of the uniaxial LC crosslinked samples manufactured from the model ($50_{MAC}50_{RM82}$, $75_{MAC}25_{RM82}$, and $90_{MAC}10_{RM82}$) and reference ($100_{MAC}0_{RM82}$) inks. All samples were aligned with the director along their long axis and had an unhindered area of 15x3 mm, with a thickness of 80±10 μm. (a) Storage modulus (E') as a function of macromer concentration, measured at 30°C above the Tg of each material (6, 15, 42 and 48°C for the materials with 100, 90, 75 and 50 wt.% of macromer content). (b) Normalized length (L/L_0) as a function of temperature during the heating process in load-bearing experiments (1 g load).

the geometry, as confirmed by Polarized Optical Microscopy (POM) (Figure S3). Gel fraction values for these LC crosslinked systems were higher than 86% for all printable inks (Figure S4). In contrast, the ink with only 25 wt.% of macromer content (75 wt.% RM82 low MW monomer) led to morphologies with no preferential alignment under the studied conditions, being this material thus discarded.

We then characterized the thermomechanical behavior of the printed samples. After printing and photopolymerization, dog-bone LC crosslinked elements (central test area 15x3 mm, 80±10 μm thickness), with their molecules oriented along the long axis of the sample, were released from their substrate to assess their dynamic mechanical properties as a function of the temperature using Dynamic Mechanical Analysis (DMA). T_g of the crosslinked LC materials was calculated at the tan δ peak. Significantly higher values than their non-polymerized precursors, as expected due to the crosslinking of the network, were identified (Figure S5). [41, 55, 56] Overall, T_g increased with increasing content of the low MW monomer constituent.

Following the approach reported by Gleeson et al., storage modulus (E') values were extracted at a relative temperature of 30°C above the T_g of each material, enabling a fair comparison of the mechanical properties across all formulations (Figure 2a) [56]. From this comparative, storage modulus increases with increasing low MW content, reaching 10, 19, 37, and 49 MPa for the materials with 100, 90, 75, and 50 wt.% of macromer content, respectively. These differences in the dynamic mechanical properties as a function of the low MW content, may be explained by higher levels of crosslinking that promote reduced chain mobility as the low MW component content increases [40, 57]. Consequently, the greatest contrast can be observed for the material $50_{MAC}50_{RM82,}$ with a significantly higher glass transition temperature (T_g at 48°C) and notably higher storage modulus, in comparison with the reference $100_{MAC}0_{RM82}$ material (T_g at 6°C), which shows the lowest storage modulus among the samples. These results highlight that adjusting the ratio of high MW main-chain macromer to low MW monomer constituent enables tailoring of the thermal and mechanical properties of 4D printed LC actuators.

Finally, the ability of these actuators to deform upon thermal stimulation in a load-bearing setting was evaluated. After applying adhesive tape to both ends of the samples, leaving an unhindered central area of 15x3 mm (80±10 μm thickness), one end was secured to the sample holder, while a 1 g steel weight was attached at the opposite end. Heating of these elements led, in all the cases, to a contraction along the longitudinal axis, parallel to the printing direction, primarily attributed to a decrease of the mesogenic order and the associated anisotropic relaxation of the aligned network. [10, 14, 15] However, the extent of contraction is highly dependent on the ratio of high to low MW constituents. For the reference material (100 wt.% macromer), a maximum contraction of 45% was observed at 120°C, as shown in Figure 2b. As the macromer content in the formulation decreases and thus the proportion of the low MW monomer constituent increases, a progressive decrease in the maximum contraction is observed. At 120°C, contractions of 18%, 7%, and 4% were observed for the LC crosslinked materials with 90, 75, and 50 wt.% of macromer content, respectively.

These variations in the maximum contractions can be explained by differences in network architecture arising from the varying ratios of high to low MW constituents used. As supported by the DMA results, a higher content of low MW monomer, which leads to a higher crosslinking density, reduces the mobility of the mesogens in the crosslinked system and limits their ability to reorient, thereby diminishing the thermally induced molecular disorder and the subsequent thermally induced deformation [58, 59]. This hypothesis is further supported by polarized optical microscopy (POM) observations of the uniaxial actuators with varying degrees of crosslinking as a function of the temperature (Figure S6). For example, the LCE system resulting from the reference $100_{MAC}0_{RM82}$ ink, therefore having the lowest degree of crosslinking, displays birefringence at low temperatures (30°C). Upon heating above 120°C, this birefringence begins to diminish, becoming the system isotropic at around 150°C. The resulting loss of mesogenic order, corresponding to randomization of molecular alignment at elevated temperatures, correlates to the associated large contraction along the preferential alignment axis. In contrast, the actuators prepared from the model formulations with progressively higher content

of the low MW monomer show reduced molecular mobility, also reflected in the POM images. The system with 90 wt.% of macromer content shows a visible drop in transmission between crossed polarizers only above 180°C, while the systems with 75 or 50 wt.% of macromer content exhibit little optical change across the entire studied temperature range, up to 210°C. Without a discernible clearing point in the range of studied temperatures, the mesogenic order of these heavily crosslinked systems is only slightly temperature-dependent, due to restricted molecular reorientation. Together, these findings explain the progressively smaller thermally induced contractions per degree of temperature change in systems with increasing crosslinking. While the mesogenic order was not directly measured in this study, the relative changes in birefringence observed by POM offer qualitative support for our interpretation, indicating that reduced optical response is consistent with restricted mesogen mobility and limited molecular reorientation. This correlation provides a valuable basis for tuning the actuation response of LC networks in stimuli responsive, load-bearing applications.

To summarize this section, the study of these model inks shows that combining high MW macromers with low MW diacrylate mesogens allows reliable printing while adjusting thermal and mechanical properties, as well as the amplitude of thermal actuation.

3 | Printable Monoacrylate-Based Ink based on Mixed Low/High Molecular Weight Constituents

Building on the blending of a high MW main-chain macromer with a low MW diacrylate monomer presented in the previous section, we extended the methodology to incorporate low MW mesogenic monoacrylates into 4D printable inks. As mentioned in the introduction, monoacrylates have been previously employed to design liquid crystal actuators responsive to stimuli such as electric fields, pH, and light, among others, often relying on surface-enforced methodologies to achieve molecular alignment [49, 60–63]. Owing to their chemical structure, however, monoacrylates possess only one reactive site and therefore act as pendant units rather than directly contributing to the network crosslinking. The presence of a single reactive group also precludes their incorporation into Michael addition–based step-growth systems, as they terminate the growing chain. For this reason, they have not been used in the preparation of macromers for direct ink writing.

In our approach, the inclusion of high MW macromers in the ink formulation is expected to provide the viscoelasticity required for extrusion and alignment needed for printing, thereby enabling the incorporation of monoacrylates into the final network without compromising printability or orientation. To explore this potential, we formulated a new ink incorporating the monoacrylate mesogen ST03866 as the low MW constituent at a concentration of 50wt.%. The same high MW macromer used for the model inks was included as the other 50 wt.% constituent (Figure 3a). This ink has been named $50_{MAC}50_{MONO}$. Finally, 3 wt.% of photoinitiator (Irgacure 819) was added to the mixture to form the printable ink.

The thermal behavior of the formulation was first characterized by DSC. T_g and $T_{LC\text{-}I}$ of the material, without the photoinitiator, were identified at −36°C and 73°C, respectively (Figure S7). This material, including the photoinitiator, was used for 4D printing. A protocol comparable to that used for the previous materials was employed: heating to 87°C for 10 min prior to each printing cycle promoted proper blending of the components and erased thermal history.

Subsequently, the printing parameters (needle diameter, temperature of the printhead and substrate, speed, and pressure) were optimized (Table S4), leading to printed lines and dog-bone samples (15x3x0.08 mm of central test dimensions) with a net alignment of the molecules in the direction of the needle movement as confirmed by POM (Figure 3b; Figure S8). Next, the printed samples were photopolymerized, obtaining minimum gel fraction values of 87%.

Thermomechanical characterization followed, with load-bearing experiments to evaluate the response under thermal stimulation. Contraction values in the longitudinal axis of the sample reached 22% upon temperatures of 120°C (Figure 3c). When comparing these results with the model material containing similar concentration of macromer ($50_{MAC}50_{RM82}$), the inclusion of monoacrylates as the low MW constituent has led to a pronounced increase of the thermally induced deformations. As highlighted earlier, monoacrylates react via a single functional group, reducing network connectivity while also increasing free volume and local chain mobility, compared to LC networks generated from diacrylates. This may account for the greater responses observed for $50_{MAC}50_{MONO.}$ The substantially larger thermo-induced contraction strains observed for monoacrylate-containing networks indicates a markedly enhanced deformability compared to the more highly crosslinked diacrylate-based systems. Overall, the study of this formulation demonstrates that the presence of a high MW macromer enables the integration of a significant fraction of monoacrylates into 4D printable inks, opening access to a wide variety of polymeric networks showing significant thermally driven deformations, and potentially accommodating other functional monomers responsive to stimuli beyond temperature.

4 | Printable Photoresponsive Ink Based on Mixed Low/High Molecular Weight Constituents

Having established that our methodology enables both diacrylate- and monoacrylate-based inks with tunable thermal response, we next examined whether it could be extended to create light-responsive systems. This extension was pursued to broaden potential applications and to demonstrate the versatility of the formulation concept. Light-responsive materials can change their shape when exposed to light, making them valuable for actuators requiring precise remote actuation [14, 15, 42, 64, 65]. By implementing the strategy presented in this work, light-responsive formulations can potentially be prepared by simply incorporating chromophores as the low MW constituent. To proof this principle, we selected a photoisomerizable azobenzene with oxygen atoms in the para positions and two acrylate end groups as the chromophore (A9A, Figure 4a). The photomechanical response of LCs containing this photoisomerizable switch has two

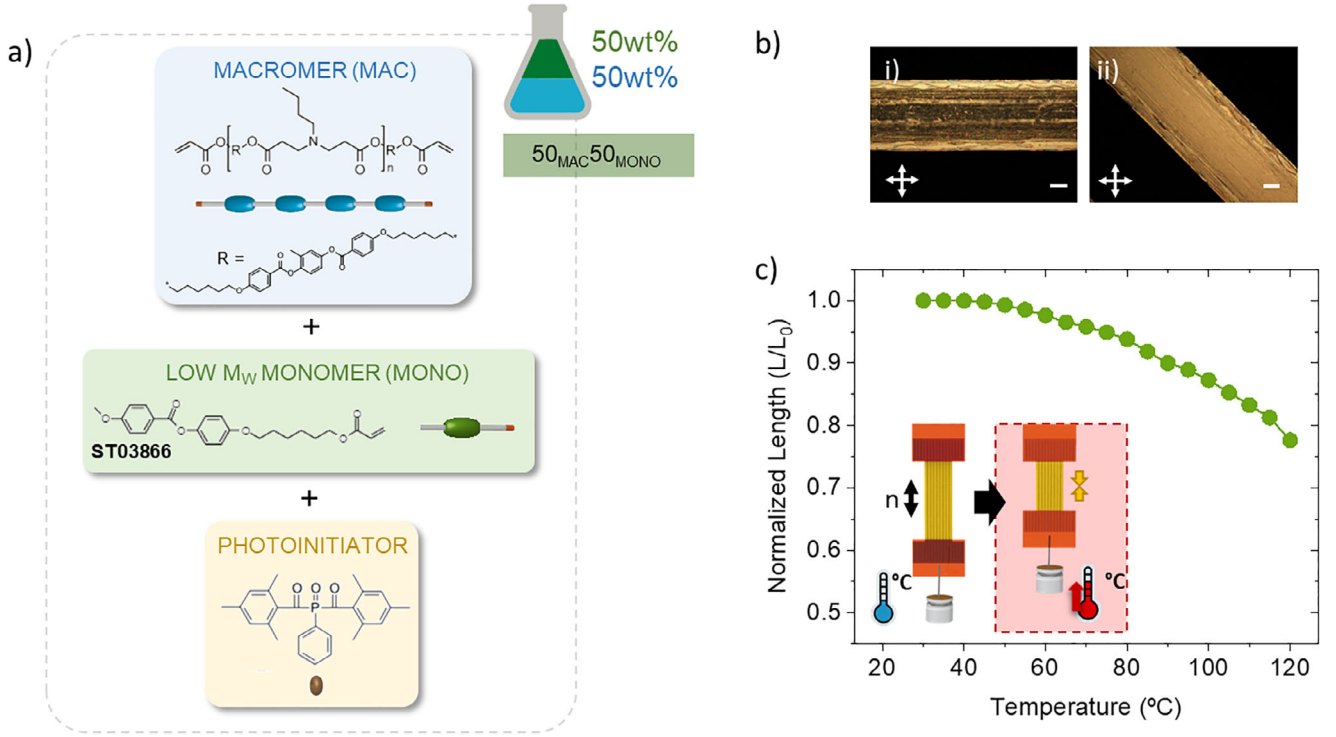

FIGURE 3 | Formulation, printing processing and response characterization of the monoacrylate-based 4D printable material. (a) Molecular constituents and relative concentration of the mixed high MW macromer (aza-Michael addition with RM82 and *n*-butylamine), low MW monoacrylate mesogen (ST03866), and photoinitiator (Irgacure 819). (b) POM images of printed lines. Lines are observed between crossed polarizers (crosses indicate polarizer transmission directions) with the printing direction oriented (i) parallel and (ii) at 45° to the first polarizer transmission direction (scale bar of 100 μm). (c) Temperature dependence of normalized length (L/L_0) of the LCs dog-bone sample in load-bearing experiments (1 g). Director along its long axis and unhindered central sample dimensions of 15x3x0.08 mm.

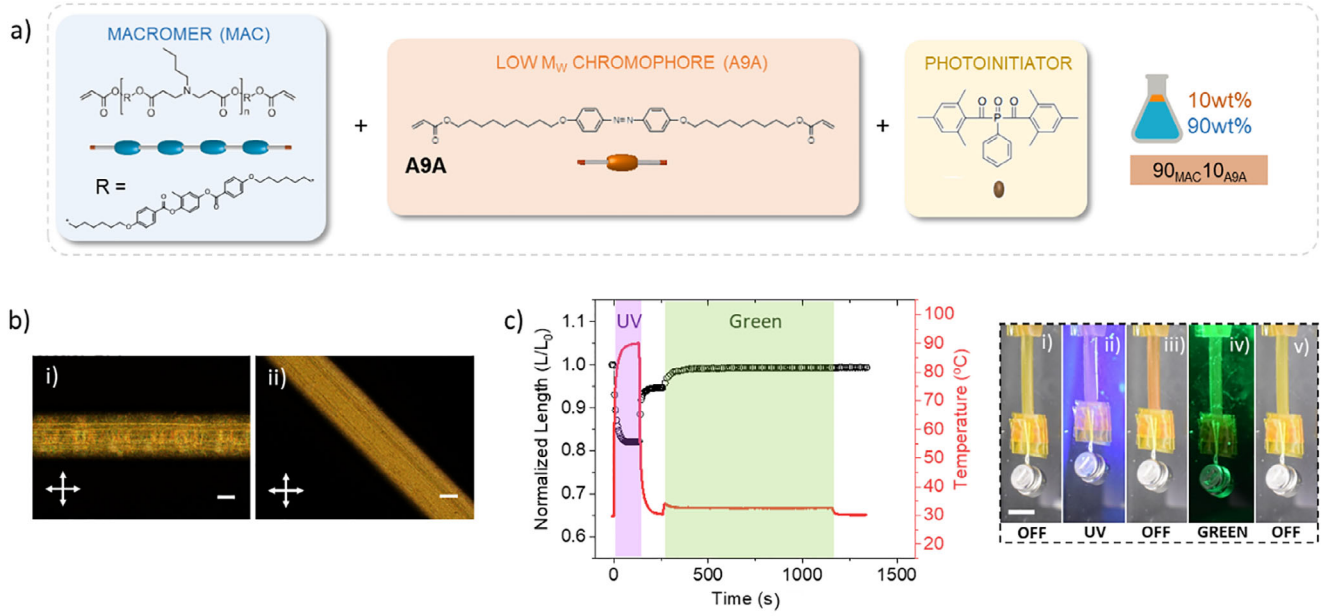

FIGURE 4 | Characterization of the synthesized azobenzene-containing printable material. (a) Schematic view of the ink components, including the high MW macromer, low MW chromophore (A9A), and photoinitiator (Irgacure 819). (b) POM images of printed lines observed between crossed polarizers (crosses indicate polarizer transmission directions) with the printing direction oriented (i) parallel and (ii) at 45° to the first polarizer transmission direction (scale bar of 100 μm). (c) Temporal dependence of the normalized length L/L_0 (black circles) of the photo-responsive LC sample and temperature (red line) during photomechanical experiments with 1 g of weight. Images show the illumination sequence: (i) before, (ii) during, and (iii) after UV illumination (200 mW cm^{-2}), as well as (iv) during and (v) after green light illumination (30 mW cm^{-2}). Scale bar of 5 mm. Director along its long axis and unhindered area of 15x3 mm, 75±5 μm thick.

contributions: photothermal and photochemical [21]. On the one hand, the photothermal contribution originates in light-induced heat generation, which leads to liquid crystal disorder and, thus, mechanical stresses like the ones described in thermomechanical systems. On the other hand, the photochemical contribution relies on the UV-induced isomerization between the *trans* and *cis* states of the azobenzene. For the azobenzene employed in this work, irradiation with UV light induces a population of *cis* isomers with a lifetime of several hours at RT. The *cis* isomer adopts a bent conformation, in comparison to the elongated, promesogenic *trans* form. Consequently, the resulting *cis* population induces a decrease in the LC order and, as a result, a measurable macroscopic mechanical response [21, 42, 61, 66].

Based on this rationale, a light-sensitive formulation has been synthesized, including 10 wt.% of A9A as the low MW constituent, thus introducing photoresponsiveness to the material (Table S5). This ink, called $90_{MAC}10_{A9A}$, includes the same high MW main-chain LC macromer (at a concentration of 90 wt.%) used for previous formulations. Additionally, 3 wt.% of photoinitiator (Irgacure 819) was added to the mixture to enable subsequent light-induced polymerization.

The phase behavior of the azobenzene-containing ink was first analyzed. In the absence of photoinitiator, DSC scans showed a clearing point ($T_{LC\text{-}I}$) at 97°C (Table S5 and Figure S9). Upon heating, a broad endothermic peak appeared at 76°C, whereas an exothermic peak was detected at 38°C during cooling. These transitions could be tentatively attributed, based on the thermal signature and known behavior of azobenzene derivatives, to the melting and crystallization of the azobenzene chromophore, respectively [65, 67]. In order to support this hypothesis, the material was analyzed under POM observation during controlled heating and cooling ramps (Figure S10). At 30°C, the material exhibits regions with a yellow and crystalline appearance, which could be tentatively attributed to phase segregated azobenzene chromophore. Upon heating, the azobenzene domains have been observed to melt and reintegrate into the LC phase, which eventually clears to an isotropic at higher temperatures.

Notably, when maintaining the material at 87°C for 10 min, reproducing similar procedure to that performed before each printing cycle in the previous materials, blending between the two components becomes apparent. When lowering the temperature back to 30°C, the initial texture is recovered, which could suggest a partial phase separation of the azobenzene from the macromer-rich matrix. This thermal behavior is consistent with the DSC thermograms. Since such behavior can affect the alignment quality and actuation reproducibility, the processing temperature has been optimized during subsequent printing and polymerization processes. Consequently, the ink was heated to a temperature of 87°C for 10 min before the printing cycle. Subsequently, the printhead was set to 75°C while the substrate was set to 50°C to prevent rapid crystallization of the material during the processing while preserving the molecular alignment of the deposited material. Thereafter, the remaining printing parameters were optimized (Table S6). Lines were first printed, and POM observation confirmed the preferential net alignment of the molecules along the needle movement direction, as well as the absence of material segregation (Figure 4b). Next, dog-bone geometries (15x3 mm of central area, 75±5 μm of thickness) for mechanical characterization were printed (Figure S11). Then, the printed samples were photopolymerized, obtaining a gel fraction value of 72%, lower than the values reached from non-azobenzene-containing systems in this work. A similar decrease in the photopolymerization efficiency has been reported by White et al. for azobenzene-containing photopolymerizable materials. This suggests that the azobenzene chromophore may interfere with the initiation or propagation steps of polymerization, either by absorbing light at the wavelength used to activate the photoinitiator or by participating in competing side reactions. [68]

The thermomechanical response of the polymerized LCs was next assessed. Samples released from the substrate contracted by a maximum of 23% under heating to 120°C with a 1 g load (Figure S12). In comparison with the model material with a similar concentration of macromer, $90_{MAC}10_{RM82}$, a slightly higher contraction has been obtained for this photo-responsive system, which could be explained by the different photopolymerization outcome, leading to a less crosslinked network capable of greater deformations.

Subsequently, and as the primary focus of this section, the response to light stimulation was explored. UV light (200 mW cm^{-2}) was applied to one side of the azobenzene-containing crosslinked LC element. As documented in the literature, illumination of free-standing uniaxial samples generally leads to bending toward the light source. This effect is caused by the gradient of light intensity across the sample thickness due to azobenzene absorption, as described by Beer's law [69–71]. To promote in-plane deformations during the light-induced contraction experiments, a weight of 1 gram was fixed to the lower end of the samples. This weight inhibits the bending deformation mode throughout the experiment and, therefore, allows for precise quantification of the dimensions of the sample over time through image analysis. A thermographic camera monitored the light-induced heating on the surface of the sample. Figure 4c shows the normalized length (L/L_0) of our photoresponsive material before, during, and after irradiation with UV light for excitation and green light for relaxation of the azobenzene chromophore. From the beginning of the UV light stimulation, light-induced heating rises until a stationary state is reached at temperatures around 90°C. In correlation with the evolution of the temperature of the sample, a contraction in the direction of the initial molecular alignment was registered, reaching a maximum value of 18%. Once UV light irradiation ceased, the temperature of the surface of the sample cooled down to RT, and the light-induced deformations decreased, reaching a slight remnant contraction (5.3 %), likely ascribed to the presence of azobenzene molecules in the *cis* state [21, 72]. The initial length of the sample was fully recovered after irradiation with green light (530 nm, 30 mW cm^{-2} for 15 min). The reversibility of the mechanical photo-induced response was confirmed upon several cycles (Figure S13). It should be noted that during UV irradiation, the photothermal and photochemical contributions to the actuation are intrinsically coupled, as temperature variations directly affect both liquid crystalline order and azobenzene isomerization kinetics, and therefore cannot be experimentally decoupled in the transient regime [21]. Nevertheless, the residual contraction observed after switching off the UV light, once thermal effects have relaxed, provides a qualitative indication of the photochemical contribution arising from the population of long-lived azobenzene *cis* isomers.

Notably, light-stimulated deformations were significantly larger than those induced thermally at similar temperatures, reaching only 9% of contraction at 90°C in thermomechanical load-bearing experiments. [21] This enhanced actuation is likely due to the photochemical contribution generated due to the azobenzene isomerization, in addition to the photothermal effect [61].

Altogether, these results show that photoactive mesogens can also be integrated into our formulation concept, expanding 4D printing toward light-responsive liquid crystalline systems.

5 | Conclusions

From thermoresponsive diacrylate- and monoacrylate-containing inks to light-responsive azobenzene systems, we demonstrated a versatile yet simple methodology to formulate 4D printable liquid crystal materials, including a significant fraction of low MW mesogens. By blending low MW constituents with high MW acrylate-ended main-chain macromers, the resulting mixtures demonstrate to be suitable for direct ink writing. Moreover, the prepared macromer, easily synthesized by the Michael addition reaction, may help to guide the molecular orientation of all constituents of the inks during the printing process. Adjustment of the ratio of macromer to low MW constituents enables a tuning of the mechanical properties and responses. Mixtures based on a blend of the high MW macromer with low MW diacrylate monomers (RM82), containing up to 50% of the low MW component, were successfully printed, giving actuators with enhanced strength and reduced thermal strain as the low MW content increased. Low MW constituents with only one reactive site, such as monoacrylates, have led to increased deformations compared to blends formulated with diacrylates at similar macromer to low MW monomer ratios.

Beyond diacrylate and monoacrylate systems, the methodology can be extended to inks incorporating functional mesogens, broadening the design space of printable actuators. Light-sensitive liquid crystal actuators, in particular, have attracted attention for their ability to generate mechanical work under remote and precise light control. In this study, we demonstrated the 4D printing of azobenzene-containing actuators, formulated with low MW azobenzene chromophores, which showed mechanical responses to both thermal and light stimulation.

Our method is also compatible with other chemically responsive mesogens as low MW units, such as those sensitive to electrical or pH changes, laying the groundwork for future research in the field of 4D printing of liquid crystal actuators with custom-made physical properties, mechanical responses, and functionalities. In particular, the incorporation of functional monoacrylates bearing polar groups, such as cyano functionalities, could provide a route to explore electrically responsive liquid crystalline networks, where the chemical functionality may be used to tailor electrical sensitivity alongside mechanical and thermomechanical properties. Furthermore, the results of this work highlight how the incorporation of low MW mesogens directly impacts ink processability, molecular alignment during printing, and the resulting actuation performance. By varying the ratio between high MW macromers and low MW monomers, we demonstrate clear transitions between printable and non-printable formulations, as well as systematic changes in actuation amplitude and network deformability. In this context, the macromer acts as an enabling component that allows otherwise unprintable low MW systems to be processed by direct ink writing, providing a complementary formulation-based design handle for tuning ink behavior and actuator performance beyond monomer chemistry alone, in line with recent formulation and processing strategies reported for printable liquid crystal elastomers [73, 74]. Altogether, this work expands the design space of 4D printable liquid crystalline systems, enabling tunable and multifunctional actuators tailored for future applications.

6 | Experimental Section

6.1 | Materials

1,4-Bis-[4-(6-acryloyloxyhexyloxy) benzoyloxy]-2-methylbenzene (RM82), 4,4'-bis(9-(acryloyloxy)nonyloxy)azobenzene (A9A), and 4-Methoxybenzoic acid 4-(6-acryloyloxy-hexyloxy)phenyl ester (ST03866) were purchased from Synthon Chemicals GmbH. Chain extender n-butylamine, photoinitiator Irgacure 819, dichloromethane (DCM) solvent, and Polyvinyl alcohol (PVA) (80 % hydrolyzed; M_w of 9,000-10,000) were purchased from Sigma Aldrich.

6.2 | Synthetic Procedure and Mixture Preparation

The macromer was synthesized via aza-Michael addition reaction, adapted from a previously reported procedure [10]. Briefly, diacrylate mesogen RM82 and n-butylamine, in a 1.02:1 molar ratio, were added into a flask and dissolved in DCM. The mixture was stirred while maintained at 40°C overnight to proceed with the reaction. After that, the mixture was redissolved in DCM to compensate from previous evaporation, and Amberlyst 15 was added to the solution to remove any trace basic residue. Subsequently, the solution was filtered and left under vacuum (100 mbar) at 40°C overnight to evaporate the solvent and obtain the high MW macromer, with near-quantitative mass recovery (>90%), calculated based on the mass of recovered material relative to the total mass of monomers introduced. The macromer was used as-prepared for subsequent ink formulation. Gel Permeation Chromatography (GPC) was performed using THF as eluent and polystyrene standards for calibration. GPC analysis was used to verify the formation of the macromer and assess its molecular weight distribution. The synthesized macromer exhibited an average molecular weight (Mw) of 8400 g·mol^{-1} and a polydispersity index (PDI) of 2.1. The corresponding GPC trace is provided in the (Figure S1).

The reference ink ($100_{MAC}0_{RM82}$) was formulated by mixing this macromer with the photoinitiator (3 wt.%), Irgacure 819, in DCM. For inks with combined high and low MW constituents, the macromer was mixed with the corresponding low MW monomer at specific ratios. Then, the photoinitiator, Irgacure 819, was added to these mixtures at a 3 wt.%. Subsequently, DCM solvent is added to dissolve and homogeneously mix all components.

These mixtures were stirred for homogeneous integration, and subsequently, the solvent was removed overnight in vacuum (100 mbar) at a temperature of 40°C.

For model thermoresponsive materials, RM82 was used as the low MW constituent. Four different model mixtures were prepared with varying macromer to RM82 ratios (90:10, 75:25, 50:50, and 25:75) expressed as a percentage of the total weight before the addition of the photoinitiator. For the monoacrylate-based material, named $50_{MAC}50_{MONO}$, the macromer was mixed with the low MW monoacrylate ST03866. Relative concentration of the macromer to the low MW monoacrylate, expressed as percentage of the total weight before the addition of the photoinitiator, was 50:50. For the photo-responsive material $90_{MAC}10_{A9A}$, 10 wt.% of azobenzene chromophore A9A was added to 90 wt.% of macromer.

6.3 | 4D Printing

Printing of the inks was performed using a home-built 3D printer as previously described, based on a computer numerically controlled (CNC) router chassis with a heated, built-in ink reservoir coupled to a needle tip [10]. Upon the application of pressure, the ink is extruded through the needle into PVA-coated glass microscope slides. Simultaneously, the needle undergoes X, Y, and Z motions. The printing direction dictates the director (n) orientation into the materials. PVA coating was prepared by applying a solution of 5 wt.% PVA and Milli-Q purified water on the glass substrates, which were then left to dry at 60°C for 60 min. Printing was controlled by WinPC-NC and CAD sample designs were generated by Libre-Cad freeware software. After printing, photopolymerization was induced by irradiation from a 300 W Mercury lamp from Oriel (Model #6286) placed in a lamp housing (Oriel, Model #66902) with a UV reflecting filter (350–450 nm, Model #66218). An additional long-pass optical filter with a cut-on wavelength of 390 nm was used for the azobenzene-containing mixture to minimize azobenzene stimulation. Despite the absence of azobenzene in the other inks, the cut-on filter was also used to standardize the procedure for all the samples. The samples were positioned 20 cm from the lamp exit, reaching an intensity of around 75 mW cm^{-2} on its surface. Curing time varied depending on the material in an effort to achieve a comparable polymerization degree throughout all materials. For the reference ink ($100_{MAC}0_{RM82}$), the total curing time was 1.5 h. For the remaining inks without azobenzene, the total curing time was 1 h. For the azobenzene-containing material total curing time was 2.5 h. For all materials, the samples were reversed every 30 min to sequentially irradiate both faces until completion of the required curing time. Curing of the model and monoacrylate-based inks was performed at RT. For the azobenzene-containing mixture, curing was performed using a heating stage at 50°C. All curing procedures were done under a mild vacuum of 100 mbars to minimize oxygen inhibition.

6.4 | General Characterization

Differential Scanning Calorimetry (DSC) measurements were conducted on all the inks, aside the photoinitiator, to determine their glass and liquid crystal-to-isotropic transition temperatures. The analysis was performed using a TA Instruments DSC Q20 system. Measurements were performed across a temperature range of −50°C to 130°C using a heating and cooling rate of 10°C min^{-1} under a nitrogen atmosphere. Exceptionally, the material $50_{MAC}50_{MONO}$ was heated up to 110°C. Third cycles were considered for the analysis. Additional phase transition analyses of the ink, aside the photoinitiator, and crosslinked LC actuators were performed with Polarized Optical Microscopy (POM) coupled to a hot-stage (Linkam LTSE420). Crosslinked LC actuators printing direction was oriented at 45° with respect to the first polarizer transmission direction. Gel Permeation Chromatography (GPC) analysis was performed in a Waters HPLC system to evaluate the average molecular weight (M_w) and polydispersity index (PDI) of the macromer, considering polystyrene as the reference material and using THF as solvent. The alignment of LC-printed samples was examined using a Polarized Optical Microscope (POM) (Nikon Eclipse 80i). The thickness of the printed elements was measured using the profilometer Bruker DektakXT Stylus Profiler.

6.5 | Gel Fraction

After curing the 4D printed samples, some of them were weighted (W_i), soaked in THF for 24 h, and then dried for 4 h in a vacuum oven at 70°C. The final weight (W_f) of the samples was measured, and the gel fraction (GF) was calculated using the following Equation (1):

$$GF\,(\%) = \frac{Wf}{Wi} x100 \tag{1}$$

6.6 | Thermo- and Photomechanical Characterization

Samples with a dog bone-shaped geometry (central area of 15x3 mm), created through extrusion printing and subsequent photopolymerization of the inks, were employed in thermo- and photo-actuated experiments. Following the photopolymerization process, the samples were submerged in water to dissolve the sacrificial PVA layer of the substrate and release the actuators. Thermomechanical characterization (E′ and tan δ) was carried out by Dynamic Mechanical Analysis (DMA) on samples of 15x3x0.08 mm using a TA Instruments Q800 apparatus in vertical tension mode. First, a preconditioning cycle was performed. Then, thermographs were obtained between −50°C and 130°C at a heating rate of 5°C min^{-1} with 0.01 N preload force, 0.5% strain, and a single 1 Hz oscillating frequency. For load-bearing experiments under thermal and light stimulation, both ends of the dog-bone samples were attached to fixation tape, leaving a rectangular testing area of 15x3 mm unhindered for actuation. Thermoactuated load-bearing experiments were performed in a homebuilt aluminium oven cavity provided with optical access allowing the observation of the deformations. The samples were held on one extreme and placed inside the oven cavity. A weight of 1 gram was attached to the lower end of the samples. Samples were heated up to 120°C and subsequently left for cooling to 30°C for several cycles in order to check the reversibility of the actuation. A thermocouple was introduced into the oven

cavity for temperature monitoring of the surroundings. Actuation on heating was monitored by acquiring images every 5°C with a digital camera Nikon D3300. For light-triggered load-bearing experiments, the samples were introduced into a metallic chamber with two opposing cyclic olefin polymer (COP) windows as optical accesses to ensure good visibility of the actuation. A small hole of 5 mm in diameter was perforated in one COP film to allow thermal monitoring of the surface of the sample using a thermographic camera (Gobi, from Xenics). One side of the sample was stimulated with a UV LED (Thorlabs, 365 nm) at 200 mW cm^{-2} for 135 s to induce *trans* to *cis* isomerization. Then, the samples were left in the dark for 2 min and, subsequently, one green LED (Thorlabs, 530 nm, 30 mW cm^{-2}) irradiated the same side of the sample for 15 min to induce azobenzene *cis* to *trans* back-isomerization. Light absorption by the COP interfaces placed between the light source and the sample was considered and corrected to reach the desired light intensities on the sample surface. Actuation of the samples was monitored by extracting images from a video recording acquired using a digital camera Nikon D3300. For load-bearing thermo- and photomechanical experiments, the length of the actuator (L) was measured from the images by drawing and measuring a line along the long axis of the central testing area of the sample, between both fixation tape ends. ImageJ free software was employed for the measurements. L is normalized by the initial length (L_0), defined as the initial length of the sample when coupled to the 1 g weight while at 30°C or before UV light irradiation, for thermo- and photomechanical load-bearing experiments, respectively.

Author Contributions

C.S.-S. conceived the concept of the ink formulation, as well as led the research and secured funding. L.C., D.L., D.J B., and C.S.-S. designed the research. L.C. and C.S.-S. conceived the materials, setups, and methodology. L.C. and M.L-V. performed the experiments and analyzed the experimental results. P.L. contributed to DMA measurements. All authors discussed the experimental results. L.C. and C.S.-S. composed the first draft. All authors reviewed and improved the initial draft and approved the final manuscript.

Acknowledgements

The described research is part of the project PRIME. This project has received funding from the European Union's Horizon 2020 research and innovation program under Grant Agreement No 829010 (PRIME). Funding had also been received from the Spanish "Ministerio de Ciencia, Innovación y Universidades (MCIU)" MICIU/AEI/10.13039/501100011033, grants PID2020-118485RB-I00 and CEX2023-001286-S, and by the European Union NextGenerationEU/PRTR. This research was also supported by CIBER- Consorcio Centro de Investigación Biomédica en Red- (CB06/01/00263), Instituto de Salud Carlos III, (Spanish Ministry of Science and Innovation and European Commission, European Regional Development Fund). This work has been supported by Gobierno de Aragón project PROY_E28_24, FEDER (EU) and Fondo Social Europeo (DGA E15_20R)., FEDER (EU) and Fondo Social Europeo (DGA E15_20R). C.S.S. acknowledges the FAB3D interdisciplinary platform (PTI-CSIC) for support. The authors acknowledge the use of the Servicios Científico-Técnicos from CEQMA (CSIC) and Servicio de Caracterización from ICTP (CSIC).

Conflicts of Interest

The authors declare no conflicts of interest.

Data Availability Statement

The data that support the findings of this study are available from the corresponding author upon reasonable request.

References

1. R. L. Truby and J. A. Lewis, "Printing Soft Matter in Three Dimensions," *Nature* 540 (2016): 371–378, https://doi.org/10.1038/nature21003.

2. J. del Barrio and C. Sánchez-Somolinos, "Light to Shape the Future: from Photolithography to 4D Printing," *Advanced Optical Materials* 7 (2019): 1900598, https://doi.org/10.1002/adom.201900598.

3. S. Tibbits, "4D Printing: Multi-Material Shape Change," *Architectural Design* 84 (2014): 116–121, https://doi.org/10.1002/ad.1710.

4. D. J. Broer and G. N. Mol, "Anisotropic Thermal Expansion of Densely Cross-Linked Oriented Polymer Networks," *Polymer Engineering & Science* 31 (1991): 625–631, https://doi.org/10.1002/pen.760310902.

5. D. J. Broer, "On the History of Reactive Mesogens: Interview with Dirk J. Broer," *Advanced Materials* 32 (2020): 1905144, https://doi.org/10.1002/adma.201905144.

6. M. Warner, "Topographic Mechanics and Applications of Liquid Crystalline Solids," *Annual Review of Condensed Matter Physics* 11 (2020): 125–145, https://doi.org/10.1146/annurev-conmatphys-031119-050738.

7. A. Rešetič, "Shape Programming of Liquid Crystal Elastomers," *Communications Chemistry* 7 (2024): 56, https://doi.org/10.1038/s42004-024-01141-2.

8. C. P. Ambulo, J. J. Burroughs, J. M. Boothby, H. Kim, M. R. Shankar, and T. H. Ware, "Four-dimensional Printing of Liquid Crystal Elastomers," *ACS Applied Materials & Interfaces* 9 (2017): 37332–37339, https://doi.org/10.1021/acsami.7b11851.

9. A. Kotikian, R. L. Truby, J. W. Boley, T. J. White, and J. A. Lewis, "3D Printing of Liquid Crystal Elastomeric Actuators with Spatially Programed Nematic Order," *Advanced Materials* 30 (2018): 1706164, https://doi.org/10.1002/adma.201706164.

10. M. López-Valdeolivas, D. Liu, and D. J. Broer, "4D Printed Actuators with Soft-Robotic Functions," *Macromolecular Rapid Communications* 39 (2018): 1700710, https://doi.org/10.1002/marc.201700710.

11. M. del Pozo, J. A. H. P. Sol, A. P. H. J. Schenning, and M. G. Debije, "4D Printing of Liquid Crystals: What's Right for Me?," *Advanced Materials* 34 (2022): 2104390, https://doi.org/10.1002/adma.202104390.

12. S. J. D. Lugger, R. M. C. Verbroekken, D. J. Mulder, and A. P. H. J. Schenning, "Direct Ink Writing of Recyclable Supramolecular Soft Actuators," *ACS Macro Letters* 11 (2022): 935–940, https://doi.org/10.1021/acsmacrolett.2c00359.

13. M. Javadzadeh, J. del Barrio, and C. Sánchez-Somolinos, "Melt Electrowriting of Liquid Crystal Elastomer Scaffolds with Programmed Mechanical Response," *Advanced Materials* 35 (2023): 2209244, https://doi.org/10.1002/adma.202209244.

14. L. Montesino, J. I. Martínez, and C. Sánchez-Somolinos, "Reprogrammable 4D Printed Liquid Crystal Elastomer Photoactuators by Means of Light-Reversible Perylene Diimide Radicals," *Advanced Functional Materials* 34 (2023): 2309019, https://doi.org/10.1002/adfm.202309019.

15. S. J. D. Lugger, L. Ceamanos, D. J. Mulder, C. Sánchez-Somolinos, and A. P. H. J. Schenning, "4D Printing of Supramolecular Liquid Crystal Elastomer Actuators Fueled by Light," *Advanced Materials Technologies* 8 (2023): 2201472, https://doi.org/10.1002/admt.202201472.

16. H. Zeng, O. M. Wani, P. Wasylczyk, and A. Priimagi, "Light-Driven, Caterpillar-Inspired Miniature Inching Robot," *Macromolecular Rapid Communications* 39 (2018): 1700224, https://doi.org/10.1002/marc.201700224.

17. Z. Deng, H. Zhang, A. Priimagi, and H. Zeng, "Light-Fueled Nonreciprocal Self-Oscillators for Fluidic Transportation and Coupling," *Advanced Materials* 36 (2024): 2209683, https://doi.org/10.1002/adma.202209683.

18. A. Kotikian, C. McMahan, E. C. Davidson, et al., "Untethered Soft Robotic Matter with Passive Control of Shape Morphing and Propulsion," *Science Robotics* 4 (2019): aax7044, https://doi.org/10.1126/scirobotics.aax7044.

19. M. del Pozo, L. Liu, M. Pilz da Cunha, et al., "Direct Ink Writing of a Light-Responsive Underwater Liquid Crystal Actuator with Atypical Temperature-Dependent Shape Changes," *Advanced Functional Materials* 30 (2020): 2005560, https://doi.org/10.1002/adfm.202005560.

20. X. Lu, C. P. Ambulo, S. Wang, et al., "4D-Printing of Photoswitchable Actuators," *Angewandte Chemie International Edition* 60 (2021): 5536–5543, https://doi.org/10.1002/anie.202012618.

21. L. Ceamanos, Z. Kahveci, M. López-Valdeolivas, D. Liu, and D. J. Broer, "Four-Dimensional Printed Liquid Crystalline Elastomer Actuators with Fast Photoinduced Mechanical Response toward Light-Driven Robotic Functions," *ACS Applied Materials & Interfaces* 12 (2020): 44195–44204, https://doi.org/10.1021/acsami.0c13341.

22. O. M. Wani, H. Zeng, and A. Priimagi, "A Light-driven Artificial Flytrap," *Nature Communications* 8 (2017): 15546, https://doi.org/10.1038/ncomms15546.

23. P. Sartori, R. S. Yadav, J. del Barrio, A. DeSimone, and C. Sánchez-Somolinos, "Photochemically Induced Propulsion of a 4D Printed Liquid Crystal Elastomer Biomimetic Swimmer," *Advanced Science* 11 (2024): 2308561, https://doi.org/10.1002/advs.202308561.

24. L. Montesino, M. López-Valdeolivas, J. I. Martínez, and C. Sánchez-Somolinos, "Bridging Sensing and Action: Autonomous Object Sorting by Reprogrammable Liquid Crystal Elastomers," *Materials Horizons* 12 (2025): 5149–5161, https://doi.org/10.1039/D5MH00498E.

25. E. R. Espíndola-Pérez, J. Campo, and C. Sánchez-Somolinos, "Multimodal and Multistimuli 4D-Printed Magnetic Composite Liquid Crystal Elastomer Actuators," *ACS Applied Materials & Interfaces* 16 (2023): 2704–2715, https://doi.org/10.1021/acsami.3c14607.

26. Y. Sun, L. Wang, Z. Zhu, et al., "A 3D-Printed Ferromagnetic Liquid Crystal Elastomer with Programmed Dual-Anisotropy and Multi-Responsiveness," *Advanced Materials* 35 (2023): 2302824, https://doi.org/10.1002/adma.202302824.

27. Y. Bai, S. Zhu, J. Liang, R. Xing, and J. Kong, "4D Printing of Magnetically Responsive Materials and Their Applications," *Research* 8 (2025): 0847, https://doi.org/10.34133/research.0847.

28. T. A. Kent, M. J. Ford, E. J. Markvicka, and C. Majidi, "Soft Actuators Using Liquid Crystal Elastomers with Encapsulated Liquid Metal Joule Heaters," *Multifunctional Materials* 3 (2020): 025003, https://doi.org/10.1088/2399-7532/ab835c.

29. C. P. Ambulo, M. J. Ford, K. Searles, C. Majidi, and T. H. Ware, "4D-Printable Liquid Metal–Liquid Crystal Elastomer Composites," *ACS Applied Materials & Interfaces* 13 (2021): 12805–12813, https://doi.org/10.1021/acsami.0c19051.

30. R. H. Volpe, D. Mistry, V. V. Patel, R. R. Patel, and C. M. Yakacki, "Dynamically Crystalizing Liquid-Crystal Elastomers for an Expandable Endplate-Conforming Interbody Fusion Cage," *Advanced Healthcare Materials* 9 (2020): 1901136, https://doi.org/10.1002/adhm.201901136.

31. A. Velasco Abadia, G. E. Bauman, T. J. White, D. K. Schwartz, and J. L. Kaar, "Direct Ink Writing of Enzyme-Containing Liquid Crystal Elastomers as Versatile Biomolecular-Responsive Actuators," *Advanced Materials Interfaces* 10 (2023): 2300086, https://doi.org/10.1002/admi.202300086.

32. J. A. H. P. Sol, H. Sentjens, L. Yang, N. Grossiord, A. P. H. J. Schenning, and M. G. Debije, "Anisotropic Iridescence and Polarization Patterns in a Direct Ink Written Chiral Photonic Polymer," *Advanced Materials* 33 (2021): 2103309, https://doi.org/10.1002/adma.202103309.

33. P. Lyu, M. O. Astam, C. Sánchez-Somolinos, and D. Liu, "Robotic Pick-and-Place Operations in Multifunctional Liquid Crystal Elastomers," *Advanced Intelligent Systems* 4 (2022): 2200280, https://doi.org/10.1002/aisy.202200280.

34. H. Zeng, O. M. Wani, P. Wasylczyk, R. Kaczmarek, and A. Priimagi, "Self-Regulating Iris Based on Light-Actuated Liquid Crystal Elastomer," *Advanced Materials* 29 (2017): 1701814, https://doi.org/10.1002/adma.201701814.

35. K. Dradrach, M. Zmyślony, Z. Deng, A. Priimagi, J. Biggins, and P. Wasylczyk, "Light-driven Peristaltic Pumping by an Actuating Splay-bend Strip," *Nature Communications* 14 (2023): 1877, https://doi.org/10.1038/s41467-023-37445-5.

36. Z. Zhang and L. Shang, "Self-Assembled Hydroxypropyl Celluloses with Structural Colors for Biomedical Applications," *Smart Medicine* 4 (2025): 70004, https://doi.org/10.1002/smmd.70004.

37. S. Gantenbein, K. Masania, W. Woigk, J. P. W. Sesseg, T. A. Tervoort, and A. R. Studart, "Three-dimensional Printing of Hierarchical Liquid-crystal-polymer Structures," *Nature* 561 (2018): 226–230, https://doi.org/10.1038/s41586-018-0474-7.

38. S. Li, Z. Song, Y. Fan, D. Wei, and Y. Liu, "Four-Dimensional Printing of Temperature-Responsive Liquid Crystal Elastomers with Programmable Shape-Changing Behavior," *Biomimetics* 8 (2023): 196, https://doi.org/10.3390/biomimetics8020196.

39. L. McDougall, J. Herman, E. Huntley, et al., "Free-Form Liquid Crystal Elastomers via Embedded 4D Printing," *ACS Applied Materials & Interfaces* 15 (2023): 58897–58904, https://doi.org/10.1021/acsami.3c14783.

40. M. O. Saed, C. P. Ambulo, H. Kim, et al., "Molecularly-Engineered, 4D-Printed Liquid Crystal Elastomer Actuators," *Advanced Functional Materials* 29 (2019): 1806412, https://doi.org/10.1002/adfm.201806412.

41. G. E. Bauman, J. M. McCracken, and T. J. White, "Actuation of Liquid Crystalline Elastomers at or below Ambient Temperature," *Angewandte Chemie—International Edition* 61 (2022): 202202577, https://doi.org/10.1002/anie.202202577.

42. L. Ceamanos, D. J. Mulder, Z. Kahveci, M. López-Valdeolivas, A. P. H. J. Schenning, and C. Sánchez-Somolinos, "Photomechanical Response under Physiological Conditions of Azobenzene-containing 4D-printed Liquid Crystal Elastomer Actuators," *Journal of Materials Chemistry B* 11 (2023): 4083–4094, https://doi.org/10.1039/D2TB02757G.

43. C. M. Yakacki, M. Saed, D. P. Nair, T. Gong, S. M. Reed, and C. N. Bowman, "Tailorable and Programmable Liquid-crystalline Elastomers Using a Two-stage Thiol-acrylate Reaction," *RSC Advances* 5 (2015): 18997–19001, https://doi.org/10.1039/c5ra01039j.

44. L. T. de Haan, C. Sánchez-Somolinos, C. M. W. Bastiaansen, A. P. H. J. Schenning, and D. J. Broer, "Engineering of Complex Order and the Macroscopic Deformation of Liquid Crystal Polymer Networks," *Angewandte Chemie* 51 (2012): 12469–12472, https://doi.org/10.1002/ange.201205964.

45. M. E. McConney, A. Martinez, V. P. Tondiglia, et al., "Topography from Topology: Photoinduced Surface Features Generated in Liquid Crystal Polymer Networks," *Advanced Materials* 25 (2013): 5880–5885, https://doi.org/10.1002/adma.201301891.

46. K. M. Herbert, H. E. Fowler, J. M. McCracken, K. R. Schlafmann, J. A. Koch, and T. J. White, "Synthesis and Alignment of Liquid Crystalline Elastomers," *Nature Reviews Materials* 7 (2021): 23–38, https://doi.org/10.1038/s41578-021-00359-z.

47. S. Li, M. Aizenberg, M. M. Lerch, and J. Aizenberg, "Programming Deformations of 3D Microstructures: Opportunities Enabled by Magnetic Alignment of Liquid Crystalline Elastomers," *Acc Mater Res* 4 (2023): 1008–1019, https://doi.org/10.1021/accountsmr.3c00101.

48. L. Gulati, C. Sánchez-Somolinos, F. Giesselmann, and P. Fischer, "Aligning and Observing the Liquid Crystal Director in 3D Using Small Magnetic Fields and a Wedge-Cell," *Advanced Functional Materials* 35 (2025): 2413513, https://doi.org/10.1002/adfm.202413513.

49. L. T. de Haan, V. Gimenez-Pinto, A. Konya, et al., "Accordion-Like Actuators of Multiple 3D Patterned Liquid Crystal Polymer Films," *Advanced Functional Materials* 24 (2014): 1251–1258, https://doi.org/10.1002/adfm.201302568.

50. T. J. White and D. J. Broer, "Programmable and Adaptive Mechanics with Liquid Crystal Polymer Networks and Elastomers," *Nature Materials* 14 (2015): 1087–1098, https://doi.org/10.1038/nmat4433.

51. G. N. Mol, K. D. Harris, C. W. M. Bastiaansen, and D. J. Broer, "Thermomechanical Responses of Liquid-crystal Networks with a Splayed Molecular Organization," *Advanced Functional Materials* 15 (2005): 1155–1159, https://doi.org/10.1002/adfm.200400503.

52. A. H. Gelebart, D. J. Mulder, M. Varga, et al., "Making Waves in a Photoactive Polymer Film," *Nature* 546 (2017): 632–636, https://doi.org/10.1038/nature22987.

53. X. Lin, W. Zou, and E. M. Terentjev, "Double Networks of Liquid-Crystalline Elastomers with Enhanced Mechanical Strength," *Macromolecules* 55 (2022): 810–820, https://doi.org/10.1021/acs.macromol.1c02065.

54. D. J. Broer, R. A. M. Hikmet, and G. Challa, "In-situ Photopolymerization of Oriented Liquid-crystalline Acrylates, 4. Influence of a Lateral Methyl Substituent on Monomer and Oriented Polymer Network Properties of a Mesogenic Diacrylate," *Die Makromolekulare Chemie* 190 (1989): 3201–3215, https://doi.org/10.1002/macp.1989.021901218.

55. M. O. Saed, A. H. Torbati, C. A. Starr, R. Visvanathan, N. A. Clark, and C. M. Yakacki, "Thiol-acrylate Main-chain Liquid-crystalline Elastomers with Tunable Thermomechanical Properties and Actuation Strain," *Journal of Polymer Science, Part B: Polymer Physics* 55 (2017): 157–168, https://doi.org/10.1002/polb.24249.

56. E. I. L. Jull, R. J. Mandle, T. Raistrick, Z. Zhang, P. J. Hine, and H. F. Gleeson, "Toward in Silico Design of Highly Tunable Liquid Crystal Elastomers," *Macromolecules* 55 (2022): 4320–4330, https://doi.org/10.1021/acs.macromol.2c00587.

57. K. M. Lee, H. Koerner, R. A. Vaia, T. J. Bunning, and T. J. White, "Relationship between the Photomechanical Response and the Thermomechanical Properties of Azobenzene Liquid Crystalline Polymer Networks," *Macromolecules* 43 (2010): 8185–8190, https://doi.org/10.1021/ma1014758.

58. D. J. Broer, J. Boven, G. N. Mol, and G. Challa, "In-situ Photopolymerization of Oriented Liquid-crystalline Acrylates, 3. Oriented Polymer Networks from a Mesogenic Diacrylate," *Die Makromolekulare Chemie* 190 (1989): 2255–2268, https://doi.org/10.1002/macp.1989.021900926.

59. C. Sánchez, B. Villacampa, R. Alcalá, et al., "Mesomorphic and Orientational Study of Materials Processed by in Situ Photopolymerization of Reactive Liquid Crystals," *Chemistry of Materials* 11 (1999): 2804–2812, https://doi.org/10.1021/cm991036x.

60. D. Liu, N. B. Tito, and D. J. Broer, "Protruding Organic Surfaces Triggered by in-plane Electric Fields," *Nature Communications* 8 (2017): 1526, https://doi.org/10.1038/s41467-017-01448-w.

61. M. P. Da Cunha, E. A. van Thoor, M. G. Debije, D. J. Broer, and A. P. H. J. Schenning, "Unravelling the Photothermal and Photomechanical Contributions to Actuation of Azobenzene-doped Liquid Crystal Polymers in Air and Water," *Journal of Materials Chemistry C* 7 (2019): 13502–13509, https://doi.org/10.1039/c9tc04440j.

62. K. D. Harris, C. W. M. Bastiaansen, J. Lub, and D. J. Broer, "Self-assembled Polymer Films for Controlled Agent-driven Motion," *Nano Letters* 5 (2005): 1857–1860, https://doi.org/10.1021/nl0514590.

63. Y. Yu, M. Nakano, and T. Ikeda, "Directed Bending of a Polymer Film by Light," *Nature* 425 (2003): 145–145, https://doi.org/10.1038/425145a.

64. M. Pilz da Cunha, M. G. Debije, and A. P. H. J. Schenning, "Bioinspired Light-driven Soft Robots Based on Liquid Crystal Polymers," *Chemical Society Reviews* 49 (2020): 6568–6578, https://doi.org/10.1039/D0CS00363H.

65. L. Liu, M. del Pozo, F. Mohseninejad, M. G. Debije, D. J. Broer, and A. P. H. J. H. J. Schenning, "Light Tracking and Light Guiding Fiber Arrays by Adjusting the Location of Photoresponsive Azobenzene in Liquid Crystal Networks," *Advanced Optical Materials* 8 (2020): 2000732, https://doi.org/10.1002/adom.202000732.

66. T. Ikeda, J. Mamiya, and Y. Yu, "Photomechanics of Liquid-Crystalline Elastomers and Other Polymers," *Angewandte Chemie International Edition* 46 (2007): 506–528, https://doi.org/10.1002/anie.200602372.

67. M.-H. Li, P. Auroy, and P. Keller, "An Azobenzene-containing Side-on Liquid Crystal Polymer," *Liquid Crystals* 27 (2000): 1497–1502, https://doi.org/10.1080/026782900750018663.

68. S. Ahn, T. H. Ware, K. M. Lee, V. P. Tondiglia, and T. J. White, "Photoinduced Topographical Feature Development in Blueprinted Azobenzene-Functionalized Liquid Crystalline Elastomers," *Advanced Functional Materials* 26 (2016): 5819–5826, https://doi.org/10.1002/adfm.201601090.

69. T. Guo, A. Svanidze, X. Zheng, and P. Palffy-Muhoray, "Regimes in the Response of Photomechanical Materials," *Applied Sciences* 12 (2022): 7723, https://doi.org/10.3390/app12157723.

70. A. Priimagi, A. Shimamura, M. Kondo, et al., "Location of the Azobenzene Moieties within the Cross-Linked Liquid-Crystalline Polymers Can Dictate the Direction of Photoinduced Bending," *ACS Macro Letters* 1 (2012): 96–99, https://doi.org/10.1021/mz200056w.

71. C. L. Van Oosten, K. D. Harris, C. W. M. Bastiaansen, and D. J. Broer, "Glassy Photomechanical Liquid-crystal Network Actuators for Microscale Devices," *European Physical Journal E* 23 (2007): 329–336, https://doi.org/10.1140/epje/i2007-10196-1.

72. S. Fredrich, T. Engels, and A. P. H. J. Schenning, "Multistable Conventional Azobenzene Liquid Crystal Actuators Using Only Visible Light: the Decisive Role of Small Amounts of Unpolymerized Monomers," *ACS Applied Polymer Materials* 4 (2022): 7751–7758, https://doi.org/10.1021/acsapm.2c01298.

73. M. J. Ford, R. Telles, D. H. Porcincula, et al., "Versatile Liquid Crystal Elastomer Formulations Using Amine-Acrylate Chemistry and Processing for Advanced Manufacturing," *ACS Applied Engineering Materials* 3 (2025): 1389–1398, https://doi.org/10.1021/acsaenm.5c00176.

74. J.-H. Lee, S. Oh, I. Jeong, et al., "Redefining the Limits of Actuating Fibers via Mesophase Control: from Contraction to Elongation," *Science Advances* 11 (2025): adt7613, https://doi.org/10.1126/sciadv.adt7613.

Supporting Information

Additional supporting information can be found online in the Supporting Information section.

Supporting File: marc70237-sup-0001-SuppMat.pdf.